RBM7 deficiency promotes breast cancer metastasis by coordinating MFGE8 splicing switch and NF-kB pathway

Fang Huang[1†], Zhenwei Dai[1†], Jinmiao Yu[1†], Kainan Wang[†2], Chaoqun Chen[1], Dan Chen[3], Jinrui Zhang[4], Mei Li[4], Jinyao Zhao[4], Wenjing Zhang[4], Xiaojie Li[5*], Yangfan Qi[4,6*], Yang Wang[1*]

[1]Sino-US Research Center for Cancer Translational Medicine of the Second Affiliated Hospital of Dalian Medical University & Institute of Cancer Stem Cell, Dalian Medical University, Dalian 116023, China

[2]Department of Oncology & Sino-US Research Center for Cancer Translational Medicine, the Second Affiliated Hospital, Dalian Medical University, Dalian 116023, China

[3]Department of Pathology, the First Affiliated Hospital of Dalian Medical University, Dalian Medical University, Dalian 116011, China

[4]Institute of Cancer Stem Cell, Dalian Medical University, Dalian 116044, China

[5]Department of Prosthodontics, College of Stomatology, Dalian Medical University, Dalian, 116044, China.

[6]Soochow University Cancer Institute, Suzhou, China

[†] These authors contributed equally to this work.

[*] Correspondence:

21 Yang Wang; Sino-US Research Center for Cancer Translational Medicine of the
22 Second Affiliated Hospital of Dalian Medical University & Institute of Cancer Stem
23 Cell, Dalian Medical University, Dalian 116023, China; Tel: +86-411-86110531;
24 Email: yangwang@dmu.edu.cn

25 Yangfan Qi; Institute of Cancer Stem Cell, Dalian Medical University, Dalian, China
26 116044; Tel: +86-411-86110531; Email: yangfanqi@dmu.edu.cn

27

28

29 Running title: RBM7 presents anti-metastasis activity by regulating splicing

30

31

32 We declare no conflict of interest on the studies described in this manuscript.

Abstract

Aberrant alternative splicing is well-known to be closely associated with tumorigenesis of various cancers. However, the intricate mechanisms underlying breast cancer metastasis driven by deregulated splicing events remain largely unexplored. Here, we unveiled RBM7 as a novel regulator of alternative splicing that plays a crucial role in counteracting the metastatic potential of breast cancer. Through bioinformatics analysis and IHC staining validation, we revealed that RNA binding motif protein 7 (RBM7) is decreased in lymph node and distant organ metastases of breast cancer as compared to primary lesions. Furthermore, we found that low expression of RBM7 is correlated with the reduced disease-free survival of breast cancer patients. Breast cancer cells with RBM7 depletion exhibited an increased potential for lung metastasis compared to scramble control cells. The absence of RBM7 stimulated breast cancer cell migration, invasion, and angiogenesis. Mechanistically, RBM7 controlled the splicing switch of MFGE8, favoring the production of the predominant isoform of MFGE8, MFGE8-L. This resulted in the attenuation of STAT1 phosphorylation and alterations in cell adhesion molecules. MFGE8-L exerted an inhibitory effect on the migratory and invasive capability of breast cancer cells, while the truncated isoform MFGE8-S, which lack the second F5/8 type C domain had the opposite effect. Particularly, the ectopic expression of MFGE8-L significantly reversed the pro-invasion effect of RBM7 silencing, but did not contribute to the promotion of angiogenesis-related secreted proteins. In RBM7-depleted cells, a gene set enrichment analysis revealed a significant

amplification of the NF-κB cascade. Concordantly, RBM7 negatively regulates p65 phosphorylation. Furthermore, an NF-κB inhibitor could obstruct the increase in HUVEC tube formation caused by RBM7 silencing. Clinically, we noticed a positive correlation between RBM7 expression and MFGE8 exon7 inclusion in breast cancer tissues. Therefore, our study not only offer mechanistic insights into how abnormal splicing contributes to the aggressiveness of breast cancer, but also provide a new approach for molecular-targeted therapy in combating breast cancer.

Keywords: RBM7; alternative splicing; breast cancer; metastasis

Introduction

Alternative splicing (AS) emerges as a substantial contributor to the production of a myriad of transcripts from limited genes, which enriched protein variation and phenotypic diversity in multicellular organisms. Pre-mRNA splicing reactions require a step-wise assembly of spliceosome, a megadalton complex that recognize consensus regulatory sequences, including 5' and 3' splice sites marking exon-intron boundary, and the branch point site (BPS), to accomplish exon definition (Shi, 2017) (Wilkinson, Charenton et al., 2020). While a splice site is suboptimal, AS emerges under control of inherent sequence acting in cis, namely exonic or intronic splicing enhancer or silence, and the cognate trans-acting splicing factors, which can strengthen or weaken the recognition of splice sites by spliceosome.

It is well documented that AS dysregulation leads to multiple human diseases, including cancer (Montes, Sanford et al., 2019) (Singh & Cooper, 2012). Tumorigenicity has been linked with cancer-specific splicing switch arising from either cis-elements mutations or deregulated splicing regulatory factors. In some cases, splicing factors, particularly spliceosomal components SF3B1 and U2AF1, are frequently mutated across diverse cancer types (Baralle, 2005) (Harbour, Roberson et al., 2013) (Smith, Choudhary et al., 2019) (Cheruiyot, Li et al., 2021). For instance, recurrent SF3B1 mutations led to retention of intronic region in BRD9 pre-mRNA, conferring loss of core subunit function to the ncBAF chromatin remodeling complex and metastatic advantage to melanoma cells (Inoue, Chew et al., 2019). Another layer of regulation involves the abnormal expression of splicing factors derived from

88 altered regulatory pathway. As an archetypal example, a set of members in SR protein
89 family such as SRSF1 and SRSF3 are upregulated in breast tumors, lung tumors,
90 glioma and exhibit oncogenic ability via altering AS products (for example, Bcl-x,
91 MYO1B, NUMB and p53) (Anczuków, Akerman et al., 2015) (Zhou, Wang et al.,
92 2019) (Tang, Horikawa et al., 2012) (Zhou, Gong et al., 2020). Otherwise, many
93 splicing factors such as RBM (RNA binding motif) proteins can either functions as
94 oncoproteins or tumor suppressors in cancer-type dependent manner (Li, Guo et al.,
95 2021), which may be attributed to tissue-specific AS patterns.

96 Breast cancer is the most common diagnosed malignancy and remain the second
97 leading cause of cancer mortality (over 41,000 deaths annually in the USA) among
98 females worldwide (Siegel, Miller et al., 2019). Metastasis to vital organs accounts for
99 approximately 90% cancer-related death. The 5-year overall survival rate of patients
100 with metastatic breast cancer is drastically decreased to about 25%, as compared to
101 the primary cancer patients' prognosis with a survival rate greater than 80% (Rabbani
102 & Mazar, 2007) (Valastyan & Weinberg, 2011). Despite advances in early diagnosis
103 and comprehensive interventions for breast cancer treatment, limited effective
104 strategy against metastasis has been an outstanding challenge for improving
105 prognostication of patients. This highlights the urgent need for deepened
106 understanding of mechanisms underlying development of metastasis. Tumor
107 metastasis is multi-step process involving a sequential cascade of events, such as
108 epithelial-mesenchymal transition (EMT), local invasion from primary tumor site,
109 lymphogenic or hematogenic dissemination, cancer cells seeding and metastatic

110 lesions formation (Liang, Zhang et al., 2020). AS dysregulation has been implicated in
111 multistage process of metastasis. For example, the switch of CD44 or FGFR2 splicing
112 isoforms can lead to EMT phenotype (Chen, Zhao et al., 2018) (Warzecha, Sato et al.,
113 2009). VEGF-A or XBP1 splicing transition is tightly linked to angiogenesis in cancer
114 (Bates, 2008) (Zeng, Xiao et al., 2013). On account of the phenotypic plasticity in
115 metastatic cells conferred by alternative splicing, further investigation in potential role
116 of critical splicing regulatory factors and the associated splicing events in breast
117 cancer metastasis is warranted.

118 RNA-binding proteins (RBPs) are a large class of conserved proteins that
119 participate in cancer development through precisely control RNA metabolism,
120 including RNA splicing. RBM7, a member of RBP family, is commonly known to
121 exert RNA surveillance activity as a component of the human nuclear exosome target
122 (NEXT) complex (Meola, Domanski et al., 2016) . Aberrant expression of RBM7 is
123 not only associated with lung fibrosis onset and motor neuronopathy, but also impacts
124 cancer cell proliferation (Fukushima, Satoh et al., 2020) (Xi, Zhang et al., 2020).
125 Previous findings have established a direct connection of RBM7 with spliceosome
126 factors SF3B2 and SF3B4 (Falk, Finogenova et al., 2016), yet whether RBM7 is
127 involved in the regulation of AS remain elusive. In this study, we report that RBM7 is
128 frequently reduced in a subset of breast cancer metastases from lymph nodes lesions
129 and distant organ as compared to primary tumors and its low expression predicts
130 dismal survival outcomes of patients. Breast cancer cells with loss of RBM7 gain
131 enhanced aggressive capability and metastatic potential. Mechanistically, RBM7

132 ablation enhanced the splicing switch of MFGE8 pre-mRNA from canonical isoform
133 MFGE8-L to a truncated isoform MFGE8-S. Ectopic expression of MFGE8-L caused
134 marked suppression of migratory and invasive ability of breast cancer cells, whereas
135 MFGE8-S showed opposite function/ disabled such function. At another layer, RBM7
136 discordantly regulated the phosphorylation of p65. In concert, NF-κB inhibitor
137 abolished pro-angiogenesis effect of RBM7 ablation in breast cancer. Above all, our
138 findings uncovered a previously unidentified role of RBM7 in breast cancer
139 metastasis via coupling MFGE8 splicing switch and NF-κB signaling activation,
140 suggesting a new therapeutic target and prognostic predictor for breast cancer.

141 **Results**

142 **RBM7 is reduced in metastatic lesions of breast cancer and positively correlated**

143 **with patients' prognosis**

144 To determine the clinical relevance of RBM7 in breast cancer, we assessed the

145 correlation between RBM7 and important clinical outcomes. Analysis of TCGA, GEO

146 and the METABRIC breast cancer datasets showed that RBM7 expression positively

147 correlates with overall survival of breast cancer patients (Figure 1A and

148 Supplementary Figure 1A-1B). RBM7 low expression predicts the reduced

149 disease-free survival in patients with breast cancer (Figure 1B and Supplementary

150 Figure 1C). Congruently, we found RBM7 is decreased in breast cancer compared to

151 normal tissues (Figure 1C and Supplementary Figure 1D). Further dissection in a

152 cohort of breast cancer patients from the cBioPortal unveiled cases with lymph node

153 metastasis have lower expression of RBM7 as compared to cases without metastasis

154 (Figure 1D). We next performed immunohistochemistry (IHC) detection of RBM7 in

155 breast cancer tissue microarrays. The results showed that patients bearing clinical

156 stage III tumors have significantly decreased RBM7 expression than patients bearing I

157 and II clinical stage tumors (Figure 1E). In tissue chip containing triple negative

158 breast cancer, the more aggressive and mesenchymal breast cancer subtype, RBM7

159 exhibits reduced protein levels in tumors as compared to paracancer tissues (Figure

160 1F). In addition, we collect specimen consisted of tumor tissues from 21 breast

161 primary cancer, in 9 cases, from metastatic loci and took advantage of IHC analysis to

162 determine the RBM7 expression. Most (25% strong positive;67% moderate positive)

163 of primary tumor samples displayed a positive IHC staining for RBM7, whereas most
164 of lung/liver metastatic lesions showed weak or negative RBM7 expression (Figure
165 1G). We also obtained paired primary breast cancer and lymph node metastatic loci
166 and found, when compared to the corresponding primary tumor, the expression of
167 RBM7 is significantly decreased in lymph node metastases (Figure 1H-1I). These
168 results associated RBM7 with breast cancer metastasis, prompting us to further
169 investigate the functional role of RBM7 in metastatic processes of breast cancer.
170

171 **RBM7 silencing provokes metastatic potential of breast cancer**

172 In light with the above findings, we generated RBM7-silenced breast cancer cells
173 using lentiviral expression of short hairpin RNA (shRNA) followed by profiling
174 high-throughput transcriptome by RNA sequencing. Strikingly, Gene Ontology and
175 pathway analysis displayed a wide range of differentially expressed genes were
176 enriched in extracellular matrix organization, cell migration and angiogenesis (Figure
177 2A-2B), which have been characterized as crucial processes in tumor metastasis. We
178 then conducted qRT-PCR analysis of theses metastasis-associated genes in
179 RBM7-depleted breast cancer cells and verified that they were up-regulated upon
180 RBM7 knockdown shown as heatmap representation (Figure 2C). The lung metastasis
181 is one of the most prevalent distant metastases that breast cancer is prone to and
182 associated with poor prognosis of patients (Medeiros & Allan, 2019). Thus, we
183 performed tail-vein transfer model to evaluate the potential impact of RBM7 on
184 pulmonary metastasis of breast cancer cells. 6×10^5 4T1 cells, the mouse breast cancer

185 cell line simulating stage IV human breast tumor, with stable RBM7 silence or control
186 vector were implanted into BALB/c mice via tail vein. RBM7-silenced 4T1 cells were
187 able to develop more spontaneous lung metastases than control cells as judged by
188 pulmonary nodules number and haematoxylin-eosin (HE) staining of lung tissues
189 (Figure 2D-2F and Supplementary Figure 2A). Cancer metastasis is comprised of a
190 complex cascade of events, such as migration, invasion and angiogenesis, thus we
191 next to determine which process is mediated by RBM7-loss in facilitating breast
192 cancer metastasis. We utilized transwell chamber with or without matrix coat and
193 would healing assays to examine the potential function of RBM7 in migration and
194 invasion capabilities and found the depletion of RBM7 led to a visible increase in
195 mobility and invasiveness of both the triple-negative breast cancer (TNBC) cell line
196 MDA-MB-231, estrogen receptor positive breast cancer cell line MCF7 and 4T1 cells
197 (Figure 2G-2H and Supplementary Figure 2B-2E). Conversely, RBM7 overexpression
198 notably repressed MDA-MB-231 and MCF7 cells to migrate or invade across
199 transwell inserts (Figure 2I-2J). Similar results were obtained in two additional TNBC
200 cell lines BT549 and HCC1937 (Supplementary Figure 2F-2G), which proved that
201 RBM7 possessed the capability to suppress the migration and invasion of breast
202 cancer cells. To examine the impact of RBM7 on angiogenesis in breast cancer, we
203 cultured human umbilical vein endothelia cells (HUVEC) with condition medium
204 obtained from culture supernatants of RBM7-depleted or scramble shRNA transduced
205 cells for tube formation analysis. Compared to the scramble control, HUVEC
206 incubated with culture medium from RBM7-knockdown breast cancer cells exhibited

207 accelerated tube formation length and branch junction (Figure 2K), suggesting the
208 inhibitory effect of RBM7 on breast cancer angiogenesis. Taken together, the above
209 data demonstrated RBM7 as tumor suppressor by regulating breast cancer migration,
210 invasion and angiogenesis.
211

212 **RBM7 exhibits splicing regulatory function in breast cancer**

213 In previous studies, RBM7 is commonly characterized as an RNA-binding
214 constituent of trimeric NEXT complex, which directs the RNA exosome to
215 non-coding transcriptome for degradation (Lubas, Andersen et al., 2015). However,
216 the mechanistical role of RBM7 in cancer remain largely unknown. Intriguingly, we
217 observed that, attributed to the ablation of RBM7, almost 551 splicing events occurred
218 significant decrease in PSI (percent spliced in), whereas 289 splicing events endured
219 increased PSI (Figure 3A). The changed events were divided among various types of
220 AS (alternative splicing), including SE (skipping exon), IR (intron retention), A5E
221 (alternative 5' splice site exon), A3E (alternative 3' splice site exon), and MXE
222 (mutually exclusive exons), of note, SE events were the most prominently regulated
223 (Figure 3B). A majority of AS events in particular of SE and A5E category were in
224 decrease of PSI upon RBM7 depletion (Figure 3C-3D), indicating that the presence of
225 RBM7 may promote the usage of alternative splice sites of SEs or A5Es.
226 Subsequently, we extracted the candidate binding motifs which reside within or near
227 cassette exons or A5E and found UUUCUU motif, simiar to RBM7 binding site
228 (polyU) were enriched in RBM7 positively regulated AS events to a greater extent

229 that control exons unimpacted by RBM7 (Figure 3E), raising the possibility that
230 RBM7 may serve as a splicing activator through directly tethering cis-element in
231 pre-mRNA. This is coherent with the nuclear localization of RBM7 in breast cancer
232 cells (Supplementary Figure 3A). In order to explore the splicing regulation activity
233 of RBM7 in distinct pre-mRNA context, we validated a series of
234 RBM7-significantly-changed splicing events across different AS types according to
235 the RNA-seq results. The RT-PCR analysis demonstrated that the PSI of selected gene
236 related to cancer progression was either increased or decreased endogenously upon
237 RBM7 depletion (Figure 3F and Supplementary Figure 3B). Considering that the AS
238 is a sophisticated multi-step reaction that is regulated by both pre-mRNA-interacting
239 splicing factor and other assistant factors in a context-dependent manner (Wright,
240 Smith et al., 2022), we doubted the divergent effect of RBM7 on distinct splicing
241 targets was due to a more complicated mechanism. Gene ontology (GO) enrichment
242 analysis identified a majority of genes undergoing AS alterations were involved in
243 cytoskeleton assembly and organization (Figure 3G). While globally analyzing the
244 network enrichment of RBM7-regulated downstream splicing events, we observed its
245 targets are functionally connected to well-linked network containing gene subgroups
246 (Figure 3H), which are associated with biological processes in tumor cell metastasis,
247 again suggesting the cancer-related function of RBM7.
248
249 **RBM7 depletion switches splicing outcomes of MFGE8 by decreasing MFGE8-L**
250 **isoform**

251 To ascertain the functional targets that explain the inhibitory role of RBM7 in
252 breast cancer metastasis, we analyzed RNA immunoprecipitation sequencing data for
253 RBM7 and whole-transcriptome sequencing data for breast cancer cells expressing
254 two shRNAs targeting RBM7. Venn diagram of 8 hub genes obtained by overlapping
255 three gene sets pointed forward a hotspot gene, namely MFGE8 (Figure 4A).
256 RNA-seq data showed that the depletion of RBM7 resulted in a significant alteration
257 in ratio of MFGE8 two isoforms, of which the canonical isoform (MFGE8-L) has
258 been demonstrated to be correlated with tumor formation and aggressiveness of breast
259 cancer (Yang, Hayashida et al., 2011). Importantly, the exon 7 located in F5/8 type C
260 2 domain, which is obligated to bind to phosphatidylserine, was lacked in the short
261 isoform of MFGE8 (MFGE8-S) (Figure 4B). Further RT-PCR identification verified
262 RBM7 ablation indeed potentiated the production of MFGE8-S in various TNBC cell
263 lines (Figure 4C). Similar results were obtained from MCF7 cells, suggesting that
264 RBM7 regulated the AS of MFGE8 independently of the ER status. In separate
265 experiments, we transfected breast cancer cells with an exogenous MFGE8 splicing
266 reporter containing exon 6-8 and 600bp of flanking intron sequences to determine the
267 splicing regulatory function of RBM7. Accordingly, the depletion of RBM7 still
268 induced the splicing shift of the minigene reporter by elevating MFGE8-S variant
269 (Figure 4D). To test whether such splicing regulatory effect was directly or indirectly,
270 we analyzed the sequence of alternative exon 7 and the motifs nearby its 5' or 3'
271 splice sites, and found two poly(U) motifs are positioned in proximal to the pseudo 3'
272 splice site. Subsequent RT-PCR assay for the precipitation in RIP assays confirmed

273 RBM7 could bind to the upstream sequence containing UUUCUU motifs adjacent to
274 3' splice site of MFGE8 cassette exon, but not another region nearby it (Figure 4E).
275 To pinpoint the location for the potential cis-element for AS regulation by RBM7, we
276 designed antisense oligonucleotides (ASOs), which have been chemically modified to
277 avoid endogenous nuclease degradation without recruiting RNase H, to block the
278 UUUCUU residues in proximity to intron6/exon7 junction. As shown in Figure 4F,
279 when compared to control ASO, treatment with ASOs targeting the potential binding
280 site (UUUCUU) of RBM7, contributed to the exclusion of exon7 of MFGE8. In
281 separate experiments, the depletion of RBM7 induced the splicing shift of the
282 minigene reporter by elevating MFGE8-S variant. While the binding motif was
283 depleted or mutated, RBM7 failed to affect the splicing outcomes of MFGE8
284 (Supplementary Figure SC). Due to its close proximity to 3' splice site, UUUCUU
285 residues bound by RBM7 might participated in spliceosome assembly on the
286 upstream 3' splice site of exon7, which may explain why disruption of the motif led
287 to almost complete exon7 skipping. Our data suggest that RBM7 regulates the exon
288 skipping of MFGE8 by directly binding to UUUCUU located at six nucleotides
289 upstream of the 3' splice-site of exon7.
290

291 **The short variant of MFGE8 abolishes the inhibitory function of its classical**
292 **isoform on breast cancer cell migration and invasion**

293 MFGE8 encodes a secreted protein, Milk fat globule-EGF factor 8 (MFG-E8),
294 which participates in a variety of cellular processes, including mammary gland

295 branching morphogenesis, angiogenesis and mucosal healing, etc (Raymond, Ensslin
296 et al., 2009). We applied MFGE8-L stably overexpressing- or depleted-breast cancer
297 cells to transwell assays and observed the cellular migratory and invasive capabilities
298 was visibly suppressed by MFGE8-L overexpression (Supplementary Figure 4A-4B).
299 On the contrary, the knockdown of MFGE8-L provoked cell migration and invasion
300 (Supplementary Figure 4C). Strikingly, while MDA-MB-231 or HCC1937 expressing
301 MFGE8-L showed a remarkable decrease in migratory and invasive ability compared
302 to control vector, MFGE8-S not only totally abolished the inhibitory function of
303 MFGE8-L but elicited modest pro-migration/ invasion actions on breast cancer cells
304 (Figure 5A and Supplementary Figure 4D-4E). We also performed Fluorescent
305 Gelatin Degradation Assays for investigating invadopodia formation and found
306 MFGE8-L up-regulation suppressed breast cancer cells invasion through a layer of
307 extracellular matrix, whereas breast cancer cells with ectopic expression of MFGE8-S
308 acquired enhanced ability to degrade matrix and invasion (Figure 5B).
309 Immunofluorescence assays revealed the MFGE8-L forms foci in cytoplasm,
310 particularly enriched near cell-cell contact sites, whereas MFGE8-S is more evenly
311 distributed in the nucleus and cytoplasm (Figure 5C). As shown in diagram of domain
312 configuration for two variants, in comparison with MFGE8-L isoform containing
313 N-terminal EGF-like domain and C-terminal twice-repeated F5/8 type C domains, the
314 protein encoded by MFGE8-S loses the second F5/8 type C domain, implying a
315 shortage of the function corresponding to membrane-binding (Supplementary Figure
316 4F). The different structural bases of two isoforms may also be linked to their distinct

317 cellular function in tumor invasion (Supplementary Figure 4G). Furthermore, we
318 compared transcriptome profiles between MFGE8-L and MFGE8-S ectopically
319 expressing breast cells and found a set of functional genes were down-regulated by
320 MFGE8-L, whereas this negative regulation was abrogated in response to MFGE8-S
321 (Supplementary Figure 4H). The differentially expressed genes between two splice
322 variants were predominantly enriched in cell adhesion molecules and JAK-STAT
323 cascade as revealed by KEGG pathway and Gene ontology analysis (Figure 5D and
324 Figure 5E). Subsequent experimental validation demonstrated that the activation of
325 STAT1 was hindered by MFGE8-L, but not affected by MFGE8-S (Figure 5F).
326 Considering that STAT1 signaling activation plays an important role in tumor cell
327 metastasis via cell adhesion molecules induction (Marimuthu, Lakshmanan et al.,
328 2022) (Chen, Hao et al., 2019), it is highly plausible that MFGE8-L, but not
329 MFGE8-S, impeded breast cancer cell motility and invasive capability in a
330 STAT1-dependent manner.
331

332 **RBM7 depletion-stimulated aggressiveness of breast cancer is dependent on**
333 **MFGE8 splicing switch and NF-kB pathway activation**

334 Next, we sought to assess if MFGE8 splicing switch is responsible for
335 acquisition of aggressive feature in RBM7-silenced breast cancer cells. Flag-tagged
336 MFGE8-L or an empty vector was co-expressed in MDA-MB-231 cells together with
337 RBM7 shRNA (Supplementary Figure 5A). Following seeding into transwell chamber,
338 cells transfected with RBM7 shRNA exerted a higher migratory and invasive

339 capability than scramble control, consistent with above data. Importantly, the
340 restoration of MFGE8-L expression diminished the acquired aggressive properties of
341 MDA-MB-231 cells resulted from RBM7 depletion (Figure 6A). Similar results were
342 obtained using RBM7-depleted MCF7 cells with or without MFGE8-L complement
343 (Figure 6A). To corroborate the role of MFGE8 splicing shift in RBM7- regulated
344 breast cancer cell invasion, we transfected triple-negative breast cancer cells with
345 ASOs directed against RBM7-binding motif and examined the potential impact on
346 cell aggressiveness. The results showed an obvious increase in exon7-skipped variant
347 as compared to the scramble negative control ASOs (Supplementary Figure 5B).
348 Meanwhile, the migrative and invasive ability of breast cancer cells treated with
349 ASOs was significantly boosted (Figure 6B), further suggesting that
350 RBM7-knockdown stimulated aggressiveness of breast cancer at least partially relies
351 on the control of MFGE8 AS. However, a series of shRBM7-upregulated secreted
352 factors that have been reported to drive tumor angiogenesis (Gopinathan, Milagre et
353 al., 2015) (Fousek, Horn et al., 2021) (Feng, Ke et al., 2019), were not impacted by
354 MFGE8-L/S (Figure 6C and Supplementary Figure 5C). Condition medium derived
355 from breast cancer cells overexpressing MFGE8-L/S showed negligible effect on
356 HUVEC tube formation (Supplementary Figure 5D, implying that there exists
357 additional mechanism underlying breast cancer metastasis attributed to RBM7
358 reduction.

359 Given that consecutive gene set enrichment analysis (GSEA) of highest-ranking
360 gene sets based on transcriptomic profile of mRNA expression showed a signature for

361 NF-κB pathway that was augmented upon depletion of RBM7 (Figure 6D), we
362 suspected that the transcriptional activation of downstream genes in NF-κB signaling
363 known to facilitate tumor angiogenesis might be involved in shRBM7-exerted
364 pro-metastatic function. As expected, the phosphorylation of p65, a core transcription
365 factor well-known to switch on NF-κB pathway, was notably enhanced by RBM7
366 knockdown. Meanwhile, IκBα phosphorylation that can blockade p65 activation was
367 curbed upon RBM7 knockdown (Figure 6E). Conversely, RBM7 overexpression
368 impeded the activation of p65 (Supplementary Figure 5E). Yet MFGE8-L/S had no
369 effect on phosphorylation of p65 or IκBα (Supplementary Figure 5F). We found
370 RBM7 depletion remarkably promoted the expression of IL-1β as judged by qPCR
371 and ELISA assays (Supplementary Figure 5G-5I). IL-1β, commonly known as a
372 pro-inflammatory cytokine, could bind to IL-1R and initiate a multistage enzymatic
373 reaction that triggers the activation of NF-κB pathway (Weber, Kracht et al., 2010)
374 (Guo, Jin et al., 2024). Thus, it is plausible the upregulation of IL-1β might be a
375 causal factor in RBM7-depletion-induced activation of NF-kB signaling. We further
376 carried out Matrigel tube formation assays and found NF-κB inhibitor PDTC
377 drastically reversed the promotion of HUVEC angiogenesis by conditional medium
378 harvested from RBM7-depleted cells (Figure 6F-6G), implying that RBM7-p65 axis
379 may participate in HUVEC angiogenesis through reprogramming the secretome of
380 breast cancer cells. Similar effect was observed with respect to cell motility and
381 invasion (Supplementary Figure 5J). Taken together, these data above indicated that
382 both MFGE8 splice switch and NF-κB pathway activation are required for mediating

383 the pro-metastasis activity of RBM7 reduction in breast cancer.

384

385 **The PSI of MFGE8 exon 7 is decreased in breast cancer patients and positively**

386 **correlated with RBM7 expression**

387 To study the clinical relevance of MFGE8 isoform switch, we analyzed the PSI

388 changes of cassette exon7 in TCGA breast cancer cohort and found exon7 skipping

389 occurs more frequently in tumor than in normal tissues (Figure 7A). Consistently, in

390 comparison with normal counterparts, the splicing of MFGE8 is shifted towards a

391 reduced proportion of MFGE8-L across multiple cancer types, including LUAD,

392 HNSC, COAD, etc (Supplementary Figure 6A). RT-PCR assay was performed in

393 surgical tumor specimens in breast cancer patients and showed increased proportion

394 of exon7 exclusion in most tumor samples when compared to normal tissues (case#1:

395 86:94; case#2: 84:86; case#3: 79:85; case#4: 63:75; case#5: 69:93; case#6: 71:80)

396 (Figure 7B). On the other hand, the lymph node metastases contain a higher

397 proportion of MFGE8 variant with skipped exon7 in comparison with paired primary

398 tumor tissues (case#1: 80:95; case#2: 86:97; case#3: 84:90; case#4: 70:78; case#5:

399 83:89) (Figure 7C). This is coherent with decreased RBM7 expression levels found in

400 breast cancer with lymph node metastasis. In addition, patients with high expression

401 of MFGE8 exon7 had a visibly better overall survival than patients with low

402 expression (Figure 7D). We performed Pearson correlation test and revealed a

403 noticeably positive correlation between the expression of RBM7 and exon7 inclusion

404 of MFGE8 in breast cancer (Figure 7E), further supporting MFGE8 isoform switch

405 regulated by RBM7.

406

407 **Discussion**

408 Previous reports have recognized the RNA-binding protein RBM7 as a
409 component of the NEXT complex that could facilitate RNA exosome targeting to a
410 subset of non-coding RNAs and aberrant transcripts (Meola et al., 2016) (Pascal
411 Preker, 2008), including short-lived exosome substrates and pre-mRNAs, for
412 surveillance and turnover . In addition to this specific characteristic, RBM7 was
413 shown to interact with subunits of 7SK snRNP complex and thus activate P-TEF
414 downstream genes in response to DNA damage (Bugai, Quaresma et al., 2019).
415 Herein, we discover a novel role of RBM7 in alternative splicing control through
416 directly binding to its cognate cis-element in pre-mRNA. Using whole-transcriptome
417 sequencing, we found the depletion of RBM7 contributed to exon exclusion in
418 approximately 70% SE/A5E events, implying RBM7 mainly functions as a splicing
419 activator in the context of SE/A5E in breast cancer. However, the increase of PSI also
420 occurred due to RBM7 knockdown in a smaller faction of splicing events, such as
421 ZMYND8. We speculated this converse impact may be associated with the
422 intrinsically sophisticated splicing processes driven by distinct core splicing factors,
423 cognate cis-acting element and co-factors in a context-dependent manner (e.g.,
424 pre-mRNA structure, base modification, antagonistic or cooperative effect of multiple
425 splicing factors). Similar to many splicing factors, like SR proteins and hnRNPs,
426 RBM7 has an RRM-domain required for target RNA recognition in the N-terminus.

427 We performed co-IP experiment and found that RBM7 could interact with RNA
428 splicing factor SF3B2, a component of spliceosomal U2 SnRNP complex
429 (Supplementary Figure 6B). Consistent with the AS regulation of MFGE8 by RBM7,
430 the depletion of SF3B2 also promoted exon7 skipping (Supplementary Figure 6C-6D),
431 implying a cooperative effect of the two proteins in regulating MFGE8 splicing. This
432 is in concert with a previous study that RRM domain of RBM7 could bind a
433 proline-rich segment within SF3B2 (Falk, Finogenova et al., 2016). The interaction
434 mode with strong similarity to $RBM7^{RRM}$–$ZCCHC8^{Proline}$ interaction in the NEXT
435 complex indicated mutually exclusive binding of SF3B2 and ZCCHC8 to RBM7.
436 Thus, RBM7 appears to play dual, but not conflicting, roles during RNA processes
437 depending on its interaction with the spliceosome or exosome.

438 Currently, the pathobiological function of RBM7 in breast cancer is
439 underexplored except one study that claimed an oncogenic role of RBM7 since its
440 knockdown inhibited breast cancer cell proliferation (Xi et al., 2020). Nevertheless, in
441 our study, RBM7 knockdown in breast cancer displayed visibly pro-metastasis
442 function with activated NF-κB signaling. More importantly, according to TCGA
443 database (total cases > 1000 used for analysis), RBM7 shows decreased expression in
444 breast cancer, particularly in the metastasis loci and has positive correlation with
445 patients' survival outcomes. It is therefore highly doubtful that RBM7 could serve as
446 an oncogene in breast cancer as previously reported. Moreover, we can't exclude
447 additional biological function of RBM7 in breast cancer. RBM7-targeted silencing for
448 breast cancer would likely be detrimental for neighbouring heathy tissue and immune

449 environment as a result of NF-κB-dependent pro-inflammatory mediators and
450 cytokines secretion. Other splicing events switch triggered by RBM7 might also be
451 linked to tumor development. For example, we found RBM7 regulated alternative
452 splicing of AKT2, which is involved in glucose metabolism (Hay, 2011). Further
453 investigation is warranted to elaborate more splicing mechanisms of RBM7 in breast
454 cancer.

455 In conclusion, we discovered that down-regulated RBM7 and its cognate
456 elevated exon7-exclusion MFGE8 were tightly related to enhanced breast cancer
457 metastatic potential and poor prognosis of patients. MFGE8-L, the canonical variant,
458 possessed the capability to trigger STAT1 phosphorylation and inhibit the motility and
459 invasion of breast cancer cells, whereas splice switch to MFGE8-S was found
460 loss-of-function for this tumor-suppressive role. At another layer, RBM7 reduction led
461 to NF-κB pathway activation, resulting in enhancement of breast tumor
462 aggressiveness. Overall, our findngs implicated that activated NF-κB pathway worked
463 in concert with MFGE8 splicing transition to spur metastasis in RBM7-depleted
464 breast cancer. Additionally, although the detailed clinical significance underlying their
465 cooperation need further in-depth investigation, we propose that RBM7 and its
466 regulated splicing variants might serve as potential therapeutic biomarker and
467 prognostic indicator in breast cancer patients.

468 **Reference**

469 Anczuków O, Akerman M, Cléry A, Wu J, Shen C, Shirole Nitin H, Raimer A, Sun S, Jensen Mads A,
470 Hua Y, Allain Frédéric HT, Krainer Adrian R (2015) SRSF1-Regulated Alternative Splicing in Breast
471 Cancer. *Molecular Cell* 60: 105-117

472 Baralle D (2005) Splicing in action: assessing disease causing sequence changes. *Journal of Medical*
473 *Genetics* 42: 737-748

474 Bates S (2008) VEGF-A splicing: the key to anti-angiogenic therapeutics? *NATURE REVIEWS* 7

475 Bugai A, Quaresma AJC, Friedel CC, Lenasi T, Düster R, Sibley CR, Fujinaga K, Kukanja P, Hennig T,
476 Blasius M, Geyer M, Ule J, Dölken L, Barborič M (2019) P-TEFb Activation by RBM7 Shapes a
477 Pro-survival Transcriptional Response to Genotoxic Stress. *Molecular Cell* 74: 254-267.e10

478 Chen C, Zhao S, Karnad A, Freeman JW (2018) The biology and role of CD44 in cancer progression:
479 therapeutic implications. *Journal of Hematology & Oncology* 11

480 Chen Y, Hao X, Sun R, Wei H, Tian Z (2019) Natural Killer Cell–Derived Interferon-Gamma Promotes
481 Hepatocellular Carcinoma Through the Epithelial Cell Adhesion Molecule–Epithelial-to-Mesenchymal
482 Transition Axis in Hepatitis B Virus Transgenic Mice. *Hepatology* 69: 1735-1750

483 Cheruiyot A, Li S, Nonavinkere Srivatsan S, Ahmed T, Chen Y, Lemacon DS, Li Y, Yang Z, Wadugu
484 BA, Warner WA, Pruett-Miller SM, Obeng EA, Link DC, He D, Xiao F, Wang X, Bailis JM, Walter MJ,
485 You Z (2021) Nonsense-Mediated RNA Decay Is a Unique Vulnerability of Cancer Cells Harboring
486 SF3B1 or U2AF1 Mutations. *Cancer Research* 81: 4499-4513

487 Falk S, Finogenova K, Melko M, Benda C, Lykke-Andersen S, Jensen TH, Conti E (2016) Structure of
488 the RBM7–ZCCHC8 core of the NEXT complex reveals connections to splicing factors. *Nature*
489 *Communications* 7

490 Feng P-C, Ke X-F, Kuang H-L, Pan L-L, Ye Q, Wu J-B (2019) RETRACTED ARTICLE: BMP2
491 secretion from hepatocellular carcinoma cell HepG2 enhances angiogenesis and tumor growth in
492 endothelial cells via activation of the MAPK/p38 signaling pathway. *Stem Cell Research & Therapy* 10
493 Fousek K, Horn LA, Palena C (2021) Interleukin-8: A chemokine at the intersection of cancer plasticity,
494 angiogenesis, and immune suppression. *Pharmacology & Therapeutics* 219
495 Fukushima K, Satoh T, Sugihara F, Sato Y, Okamoto T, Mitsui Y, Yoshio S, Li S, Nojima S, Motooka D,
496 Nakamura S, Kida H, Standley DM, Morii E, Kanto T, Yanagita M, Matsuura Y, Nagasawa T,
497 Kumanogoh A, Akira S (2020) Dysregulated Expression of the Nuclear Exosome Targeting Complex
498 Component Rbm7 in Nonhematopoietic Cells Licenses the Development of Fibrosis. *Immunity* 52:
499 542-556.e13
500 Gopinathan G, Milagre C, Pearce OMT, Reynolds LE, Hodivala-Dilke K, Leinster DA, Zhong H,
501 Hollingsworth RE, Thompson R, Whiteford JR, Balkwill F (2015) Interleukin-6 Stimulates Defective
502 Angiogenesis. *Cancer Research* 75: 3098-3107
503 Harbour JW, Roberson EDO, Anbunathan H, Onken MD, Worley LA, Bowcock AM (2013) Recurrent
504 mutations at codon 625 of the splicing factor SF3B1 in uveal melanoma. *Nature Genetics* 45: 133-135
505 Hay N (2011) Akt isoforms and glucose homeostasis – the leptin connection. *Trends in Endocrinology*
506 *& Metabolism* 22: 66-73
507 Inoue D, Chew G-L, Liu B, Michel BC, Pangallo J, D'Avino AR, Hitchman T, North K, Lee SC-W,
508 Bitner L, Block A, Moore AR, Yoshimi A, Escobar-Hoyos L, Cho H, Penson A, Lu SX, Taylor J, Chen
509 Y, Kadoch C et al. (2019) Spliceosomal disruption of the non-canonical BAF complex in cancer.
510 *Nature* 574: 432-436
511 Li Z, Guo Q, Zhang J, Fu Z, Wang Y, Wang T, Tang J (2021) The RNA-Binding Motif Protein Family

512 in Cancer: Friend or Foe? *Frontiers in Oncology* 11

513 Liang Y, Zhang H, Song X, Yang Q (2020) Metastatic heterogeneity of breast cancer: Molecular

514 mechanism and potential therapeutic targets. *Seminars in Cancer Biology* 60: 14-27

515 Lubas M, Andersen Peter R, Schein A, Dziembowski A, Kudla G, Jensen Torben H (2015) The Human

516 Nuclear Exosome Targeting Complex Is Loaded onto Newly Synthesized RNA to Direct Early

517 Ribonucleolysis. *Cell Reports* 10: 178-192

518 Marimuthu S, Lakshmanan I, Muniyan S, Gautam SK, Nimmakayala RK, Rauth S, Atri P, Shah A,

519 Bhyravbhatla N, Mallya K, Grandgenett PM, Hollingsworth MA, Datta K, Jain M, Ponnusamy MP,

520 Batra SK (2022) MUC16 Promotes Liver Metastasis of Pancreatic Ductal Adenocarcinoma by

521 Upregulating NRP2-Associated Cell Adhesion. *Molecular Cancer Research* 20: 1208-1221

522 Medeiros B, Allan AL (2019) Molecular Mechanisms of Breast Cancer Metastasis to the Lung: Clinical

523 and Experimental Perspectives. *International Journal of Molecular Sciences* 20

524 Meola N, Domanski M, Karadoulama E, Chen Y, Gentil C, Pultz D, Vitting-Seerup K, Lykke-Andersen

525 S, Andersen Jens S, Sandelin A, Jensen Torben H (2016) Identification of a Nuclear Exosome Decay

526 Pathway for Processed Transcripts. *Molecular Cell* 64: 520-533

527 Montes M, Sanford BL, Comiskey DF, Chandler DS (2019) RNA Splicing and Disease: Animal

528 Models to Therapies. *Trends in Genetics* 35: 68-87

529 Pascal Preker JN, Susanne Kammler, Søren Lykke-Andersen, Marianne S. Christensen, Christophe K.

530 Mapendano, Mikkel H. Schierup, Torben Heick Jensen (2008) RNA Exosome Depletion Reveals

531 Transcription Upstream of Active Human Promoters. *SCIENCE* 322: 4

532 Rabbani SA, Mazar AP (2007) Evaluating distant metastases in breast cancer: from biology to

533 outcomes. *Cancer and Metastasis Reviews* 26: 663-674

534 Raymond A, Ensslin MA, Shur BD (2009) SED1/MFG-E8: A Bi-Motif protein that orchestrates diverse
535 cellular interactions. *Journal of Cellular Biochemistry* 106: 957-966
536 Shi Y (2017) Mechanistic insights into precursor messenger RNA splicing by the spliceosome. *Nature*
537 *Reviews Molecular Cell Biology* 18: 655-670
538 Siegel RL, Miller KD, Jemal A (2019) Cancer statistics, 2019. *CA: A Cancer Journal for Clinicians* 69:
539 7-34
540 Singh RK, Cooper TA (2012) Pre-mRNA splicing in disease and therapeutics. *Trends in Molecular*
541 *Medicine* 18: 472-482
542 Smith MA, Choudhary GS, Pellagatti A, Choi K, Bolanos LC, Bhagat TD, Gordon-Mitchell S, Von
543 Ahrens D, Pradhan K, Steeples V, Kim S, Steidl U, Walter M, Fraser IDC, Kulkarni A, Salomonis N,
544 Komurov K, Boultwood J, Verma A, Starczynowski DT (2019) U2AF1 mutations induce oncogenic
545 IRAK4 isoforms and activate innate immune pathways in myeloid malignancies. *Nature Cell Biology*
546 21: 640-650
547 Tang Y, Horikawa I, Ajiro M, Robles AI, Fujita K, Mondal AM, Stauffer JK, Zheng ZM, Harris CC
548 (2012) Downregulation of splicing factor SRSF3 induces p53β, an alternatively spliced isoform of p53
549 that promotes cellular senescence. *Oncogene* 32: 2792-2798
550 Valastyan S, Weinberg Robert A (2011) Tumor Metastasis: Molecular Insights and Evolving Paradigms.
551 *Cell* 147: 275-292
552 Warzecha CC, Sato TK, Nabet B, Hogenesch JB, Carstens RP (2009) ESRP1 and ESRP2 Are Epithelial
553 Cell-Type-Specific Regulators of FGFR2 Splicing. *Molecular Cell* 33: 591-601
554 Wilkinson ME, Charenton C, Nagai K (2020) RNA Splicing by the Spliceosome. *Annual Review of*
555 *Biochemistry* 89: 359-388

556 Wright CJ, Smith CWJ, Jiggins CD (2022) Alternative splicing as a source of phenotypic diversity.
557 *Nature Reviews Genetics* 23: 697-710
558 Xi P-W, Zhang X, Zhu L, Dai X-Y, Cheng L, Hu Y, Shi L, Wei J-F, Ding Q (2020) Oncogenic action of
559 the exosome cofactor RBM7 by stabilization of CDK1 mRNA in breast cancer. *npj Breast Cancer* 6
560 Yang C, Hayashida T, Forster N, Li C, Shen D, Maheswaran S, Chen L, Anderson KS, Ellisen LW,
561 Sgroi D, Schmidt EV (2011) The Integrin αvβ3-5 Ligand MFG-E8 Is a p63/p73 Target Gene in
562 Triple-Negative Breast Cancers but Exhibits Suppressive Functions in ER+ and erbB2+ Breast Cancers.
563 *Cancer Research* 71: 937-945
564 Zeng L, Xiao Q, Chen M, Margariti A, Martin D, Ivetic A, Xu H, Mason J, Wang W, Cockerill G, Mori
565 K, Li JY-s, Chien S, Hu Y, Xu Q (2013) Vascular Endothelial Cell Growth–Activated XBP1 Splicing in
566 Endothelial Cells Is Crucial for Angiogenesis. *Circulation* 127: 1712-1722
567 Zhou X, Wang R, Li X, Yu L, Hua D, Sun C, Shi C, Luo W, Rao C, Jiang Z, Feng Y, Wang Q, Yu S
568 (2019) Splicing factor SRSF1 promotes gliomagenesis via oncogenic splice-switching of MYO1B.
569 *Journal of Clinical Investigation* 129: 676-693
570 Zhou Z, Gong Q, Lin Z, Wang Y, Li M, Wang L, Ding H, Li P (2020) Emerging Roles of SRSF3 as a
571 Therapeutic Target for Cancer. *Frontiers in Oncology* 10
572 Axel Weber PW, Michael Kracht* (2010) Interleukin-1 (IL-1) Pathway. SCIENCESIGNALING 3:105
573 Guo Q, Jin Y, Chen X, Ye X, Shen X, Lin M, Zeng C, Zhou T and Zhang J (2024) NF-κB in biology
574 and targeted therapy: new insights and translational implications. Signal Transduction and Targeted
575 Therapy 9:53
576
577

578 **Materials and Methods**

579 **Cell culture**

580 Human breast cancer cell lines (MDA-MB-231, MCF7, HCC1937 and BT-549) and
581 human embryonic kidney cell HEK293T in this article were obtained from the
582 American Type Culture Collection (ATCC). MDA-MB-231 cells were cultured
583 without carbon dioxide at 37℃ in Leibovitz's L-15 medium (Gibco) contained 10%
584 FBS (SINSAGE TECH). MCF7 and HEK293T cells were cultured with DMEM
585 mediun (Gibco) supplemented with 10% FBS. HCC1937 cells were cultured with
586 RPMI-1640 media (Gibco) supplemented with 10% FBS, while BT-549 was
587 maintained with RPMI-1640 media (Gibco) supplemented with 10% FBS and 0.023
588 U/ml insulin. HUVECs were cultured with Endothelial Cell Medium (ScienCell)
589 supplemented with ECGS (ScienCell), P/S solution (ScienCell) and 10% FBS
590 (ScienCell). Except for MDA-MB-231, all the cells above were cultured in a 37 °C
591 humidified incubator.

592 **Stable breast cancer cell lines construction**

593 To generate RBM7 overexpression vector, its coding regions (NM_016090.4) were
594 cloned into pCDH-CMV-MCS-EF1-Puro with N-terminal Flag tag or HA-tag.To
595 construct MFGE8-L/S vectors, the coding regions of MFGE8-L (NM_005928.4) and
596 MFGE8-S (NM_001114614.3) were cloned into pCDH-CMV-MCS-EF1-Puro with
597 N-terminal Flag tag. For RBM7 knockdown, target-specific shRNA (RBM7-sh1:
598 5'-CGAAAGGACTATGGATAACAT-3';RBM7-sh2:5'-CTACCTAGCAGATAGACA
599 TTA-3') was cloned into pLKO.1 vector. And HEK293T cells were transfected these
600 over-expression (or low-expression) lentivirus plasmisd together with lentivirus
601 packaging plasmids pPAX2 and pMD2 according to the manufacturer's instructions.
602 Viruses were collected 48 hours after transfection and then to infect breast cancer cell
603 line with 8 ug/ml polybrene (beyotime biotechnology) for 24 hours. Positive cells
604 were selected with 3 ug/ml puromycin.

605 **Western Blot assay**

606 Cells were lysed with RIPA buffer (10 mM Tris-HCl pH 7.5, 150 mM NaCl, 0.1%
607 SDS, 1% Triton X-100, and 1% sodium deoxycholate) supplemented with protein
608 tyrosine phosphatase inhibitor Na_3VO_4 (1mM), serine protease inhibitor PMSF (1mM)
609 and protease inhibitor Cocktail. Immunoblotting assay was performed using standard
610 methods. The following antibodies were used: anti-RBM7 (Sigma-Aldrich,
611 HPA013993), anti-Flag (Sigma-Aldrich, F1804), anti-GAPDH (Proteintech,
612 10494-1-AP), anti-α-Tubulin (Proteintech, 11224-1-AP), anti-HA tag (Abcam,
613 ab9110), anti-Phospho-NF-κB p65 (Cell Signaling Technology, #3033), anti-NF-κB
614 p65 (Cell Signaling Technology, #8242), anti-IκBα (Cell Signaling Technology,
615 #4814), anti-Phospho-IκBα (Ser32) (Cell Signaling Technology, #2859),
616 anti-Phospho-stat1 (Tyr701) (Cell Signaling Technology, #8062), and anti-MFGE8
617 (R&D systems, MAB2767). The protein bands were detected with ECL enhanced
618 chemiluminescence regent kits (NCM, Biotech), visualized using the MiniChemi™
619 Cheminescent image system (Beijing Sage Creation, China).

620 **RNA isolation, RNA sequencing, and PCR**

621 Total RNA from cells and tumor tissues was extracted using Trizol (Invitrogen)
622 according to the manufacturer's instructions. Total mRNA was cleaned up using
623 RNeasy Lipid Tissue Mini Kit (Qiagen, USA). And RNA-seq was carried out on
624 platform of Novogene Illumina sequencing. cDNAs were obtained using *Evo M-MLV*
625 Plus 1st Strand cDNA Synthesis Kit (Accurate Biotechnology, AG11615) with
626 random primers. qRT-PCR was carried out using MonAmp™ Universal ChemoHS
627 Specificity Plus qPCR Mix. GAPDH mRNA was examined as control for
628 normalization. Gene expression relative to GAPDH was calculated using the formula
629 $2^{-\Delta\Delta CT}$. For identified alternative splicing events, primers of the upstream and
630 downstream of variable exons or introns were designed and PCR assay was performed.
631 PCR products were subject to DNA agarose gel electrophoresis. AS events change of
632 percent-spliced-in (PSI) values were the ratio of retained splices to total transcripts.
633 The amount of each splicing isoform was measured with ImageJ. All the primers are
634 showed in Table1.

635 **Migration and invasion assays**

636 For transwell migration assay, 10×10^4 MDA-MB-231 or other breast cancer cells
637 (MCF7, BT-549 and HCC1937) were plated in the upper chamber of 6.5 mm insert
638 (Costar, USA) with 8.0 μm polycarbonate membrane with 100 μL serum-free medium.
639 For invasion assay, 10×10^4 breast cancer cells were seeded in the top chamber of
640 each Matrigel-coated insert (BD Biosciences, USA). After 24 hours or 48 hours of
641 incubation at 37 °C, migrated or invaded cells were fixed with 4% PFA and stained in
642 0.1% crystal violet. The cell number was counted by ImageJ software in 3 views from
643 3 independent experiments.

644 **Wound healing**

645 Knockdown RBM7 in MDA-MB-231 and 4T1 cells or control cells were implanted
646 into 6-well culture dishes. When the cells grew about 90% confluence, lines of the
647 same width were drawn on the bottom of the culture dish using autoclaved sterile tips.
648 Images were captured at 0 and 36 hours after the wounding. Data shown were
649 representative of three independent repeats.

650 **Gelatin Degradation Assay**

651 To evaluate the ability of breast cancer cells to form invadopodia and degrade matrix,
652 QCM Gelatin Invadopodia Assay (ECM670-1, Merck Millipore) was performed
653 according to the manufacturers' protocol. Briefly, 1×10^4 MFGE8-L/S-overexpressing
654 or control MDA-MB-231 cells were suspended in L-15 medium with 10% FBS and
655 seeded into the pre-treated 96-well plate. After 48 hours, the cells were washed twice
656 with PBS. Fix cells with 3.7% formaldehyde for 30 minutes. Then these cells were
657 stained respectively with TRITC-phalloidin and DAPI for 1 hour. The ability of cells
658 to degrade the matrix was imaged using immunofluorescence microscopy (LEICA
659 DMi8, Germany) and the area of invadopodia was measured using the Image J
660 software.

661 **Tube formation of HUVECs assay**

662 Capillary tube formation assay was used to observe angiogenesis of HUVECs.
663 HUVECs were seeded into 48-well plate coated with growth factor reduced Matrigel
664 (BD Biosciences). HUVECs cells were treated with conditioned medium for 4-5

665 hours and then formation of capillary-like tubes was observed and stained with
666 calcein for 30 minutes. Images of blood vessels were taken using fluorescence
667 microscopy. And the tube length was analyzed by ImageJ software.

668 **Immunofluorescence assay**

669 After seeded on coverslips for 36 hours, the MDA-MB-231 cells were immersion
670 fixed with 4% PFA for 20 minutes at room temperature, washed 3 times in PBS. Then
671 the cells were treated with 0.2 % Triton-X100 in PBS for 10 minutes and blocked with
672 3% BSA for 10 minutes. Next the cells were immersed in primary antibody at 4℃
673 overnight, washed in PBS 3 times for 5 minutes each, and incubated with secondary
674 antibody labelled with Alexa fluorophore 488/592 for 1 hour at RT. After washing 3
675 times in PBS, the cells were dyed with DAPI. In addition, antibodies targeting RBM7
676 (Sigma, HPA013993), and Flag (Sigma, 3165) were used in the assay. The pictures
677 are captured with fluorescent microscope (Leica, USA).

678 **RNA immunoprecipitation assay**

679 RNA immunoprecipitation was performed as previously described. In brief,
680 HEK293T cells were transfected Flag-RBM7 or control plasmid. After 48 hours of
681 transfection, Flag-RBM7 or control cells were collected and cross-linked by 1%
682 formaldehyde, homogenized in lysis buffer (50 mM Tris-HCl Ph 7.5, 0.4 M NaCl, 1
683 mM EDTA, 1mM DTT, 0.5% TritonX-100, 10% Glycerol supplemented with RNase
684 inhibitor and broad-spectrum protease inhibitors Cocktail), and broke with an
685 ultrasonic crusher. And solubilized cell lysate was obtained and precleared by
686 ProteinG-agarose beads together with nonspecific tRNA to remove nonspecific
687 binding. Then binding RNAs with RBM7 protein were precipitated with Anti-Flag
688 M2 Affinity beads. Co-precipitated RNAs were subject to RT-PCR. Input controls
689 (total RNAs) and Flag-controls were assayed simultaneously to prove that the
690 detected signals were the result of RNAs specifically binding to RBM7. The
691 gene-specific primers were designed MFGE8-RIP1-F:5'-tatttatgccccctcaccgc-3';
692 MFGE8-RIP1-R:5'-atggtggctgcctgtaat-3';MFGE8-RIP2-F:5'-ctgaggctcacccaagtag-3';
693 MFGE8-RIP2-R:5'-GTAGGATGCCACAAACTG-3'). GAPDH mRNA was as
694 negative control (GAPDH-F 5'-GGGGAAGGTGAAGGTCG-G-3'; GAPDH-R
695 5'-TTGAGGTCAATGAAGGGG-3').

696 **Antisense oligonucleotide (ASO)-mediated splicing blockade**

697 MFGE8-ASOs were synthesized with a full-length phosphorothioate backbone and
698 2'-O-methyl modified ribose molecules (GenScriptBiotech Corp). ASO was
699 transfected at final concentration of 500 nM using Lipofectamine3000 (Thermo Fisher
700 Scientific) according to the manufacturer's instructions. The MCF7 cells were
701 harvested for RNA and splicing assays 48 h after transfection.

702 **Animal experiments**

703 All procedures and experimental protocols involving mice were approved by the
704 Institutional Animal Care and Use Committee (IACUC) of Dalian Medical University.
705 Female BALB/C mice (6 weeks old, 4-5 mice per group as indicated in figures and/or
706 figure legends) were injected into tail vein with murine 4T1 breast cancer cells (6 ×
707 10^5 cells) to develop mice model of pulmonary metastasis. After about 3 weeks, all
708 mice were euthanized, and lungs were harvested, fixed and paraffin embedded. After

lungs were H&E stained, the number of metastatic lesions were enumerated by pathologist using brightfield microscopy.

Clinical tissues samples collection

All human breast cancer tissues or normal tissue were obtained with written informed consent from patients or their guardians prior to participation in the study. The Institutional Review Board of the Dalian Medical University approved use of the tumor specimens in this study.

Bioinformatics analysis

RBM7 expression data and survival data (including OS and DFS) were obtained from the METABRIC database using the Cbioportal web tool. Based on the expression level of RBM7, the patients were divided into four categories (i.e., Q1, Q2, Q3, Q4) by quartiles, and then log-rank was employed to compare the survival differences of patients in different categories. Cbioportal cited (Cerami E et al. The cBio cancer genomics portal: an open platform for exploring multidimensional cancer genomics data. Cancer Discov. 2012 May;2(5):401-4). Through the analysis of alternative splicing events in RBM7 knocked-down MDA-MB-231 cells compared to control, exon skipping events were screened out, and then selected the sequence of the 500nt region upstream of the alternative exon for subsequent base sequence enrichment analysis. The XSTREME tool provided by the online tool meme-suite (https://meme-suite.org/meme/) was used to perform Motif Discovery and Enrichment Analysis. E-value < 0.05 as the significance standard to output the results.

Statistical analyses

Statistical analyses and statistical graphs were conducted by GraphPad Prism 8 software. To compare the differences between the two variables, Student's T-test, one-way ANOVA with Dunnett multiple comparisons, and one-way ANOVA with Tukey's multiple comparisons according to the specific situation were applied. $*P < 0.05$, $**P < 0.01$, $***P < 0.001$, and $****P < 0.0001$ indicated the significant difference.

Data availability

The authors declare that all the data supporting the findings of this study are available within the article and its supplementary information files. RNA-seq data in this study have been deposited in Gene Expression Omnibus of NCBI with the accession code GSE248938.

Author contributions

YW and YQ conceived the project and designed the experiments. FH, JY, ZD, KW, and DC performed most of the experiments, whereas CC, JZhang, JZhao and WZ performed data analysis. YW and YQ wrote the manuscript. DC, XL, ML performed writing-review and editing.

These authors FH, ZD, JY, KW contributed equally to this work.

Acknowledgements

This work was supported by the National Key R&D Program of China (2022YFA1104002, 2023YFE0117500 to YW); the National Natural Science Foundation of China (82225034, 81830088 to YW; 82103148 to YQ; 82273427 to WZ); the Science and Technology Innovation Foundation of Dalian (2022JJ11CG009 to YW), Liaoning Revitalization Talents Program (XLYC2202027 to YW); Interdisciplinary Research Cooperation Project Team Funding of Dalian Medical University (JCHZ2023008 to YQ); Joint Research Program of Natural Science Foundation of Liaoning, China (2023-MSLH-023 to YQ); the Science and Technology Innovation Talent Support Program of Dalian (2022RQ056 YQ); Dalian High Level Talents Renovation Supporting Program (2022RJ15 to WZ).

Study Approval

The Institutional Animal Care and Use Committee of the Dalian Medical University approved use of animal models in this study. All human tumor tissues were obtained with written informed consent from patients or their guardians prior to participation in the study. The Institutional Review Board of the Dalian Medical University approved use of the tumor specimens in this study.

766 **Figures and figure legends**

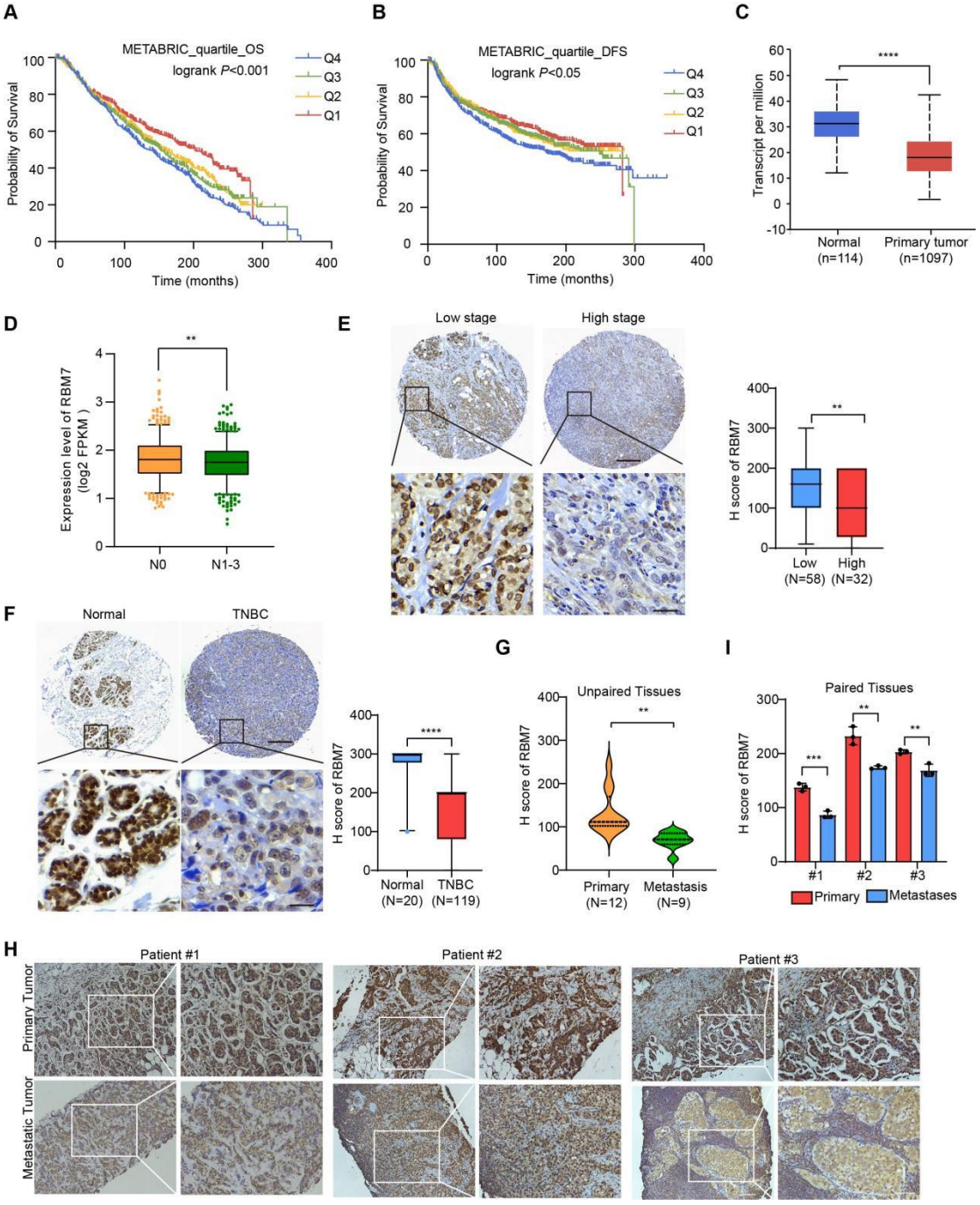

767 **Figure 1. Decreased RBM7 expression was associated with poor prognosis of**
768 **breast cancer.** (A-B) The correlation between RBM7 mRNA expression and overall
769 survival (OS) or disease-free-survival (DFS) of breast cancer patients (n=1980) was
770 analyzed based on the METABRIC dataset. The samples were divided into four equal
771 parts, containing lower quartile Q1, median quartile Q2, upper quartile Q3 and higher
772 quartile Q4 according to the expression of RBM7. Data are presented as means ± SD

773 and *P* values were obtained by Mantel-Cox log-rank test. (C) The expression of
774 RBM7 in primary breast carcinoma (n=1097) compared to normal tissues (n=114)
775 was analyzed through UALCAN dataset. (D) Analysis of RBM7 expression in breast
776 cancer lymph node metastases in comparison with breast cancer tissues with no lymph
777 node metastasis based on TCGA dataset. BRCA samples were classified into N0 (No
778 regional lymph node involvement) (n=515), and metastases in lymph node (N1-N3)
779 (n=565). (E) Representative IHC images of RBM7 staining for patients at high (n=32)
780 or low (n=58) clinical stages on tissue microarray of breast cancer specimens. Scale
781 bars = 300 μm (top) or 30 μm (bottom). (F) Representative images of the IHC staining
782 of RBM7 in a tissue microarray containing triple-negative breast cancer (n=119) and
783 para-carcinoma tissues (n=20). Scale bars = 300 μm (top) and 30 μm (bottom). (G)
784 Quantitative analysis of RBM7 expression according to IHC staining scores in
785 primary breast cancer (n=12) and distant metastases (breast cancer lung metastases,
786 n=4; breast cancer liver metastases, n=5). (H-I) Representative IHC images and
787 quantitative analyses for RBM7 staining in 3 paired primary breast cancer and
788 lymphatic metastases are shown. Scale bar = 100 μm. Data are presented as means ±
789 SD and *P* values were obtained by unpaired Student's t test (C-I). $^{**}P < 0.01$, $^{***}P <$
790 0.001, $^{****}P < 0.0001$.
791

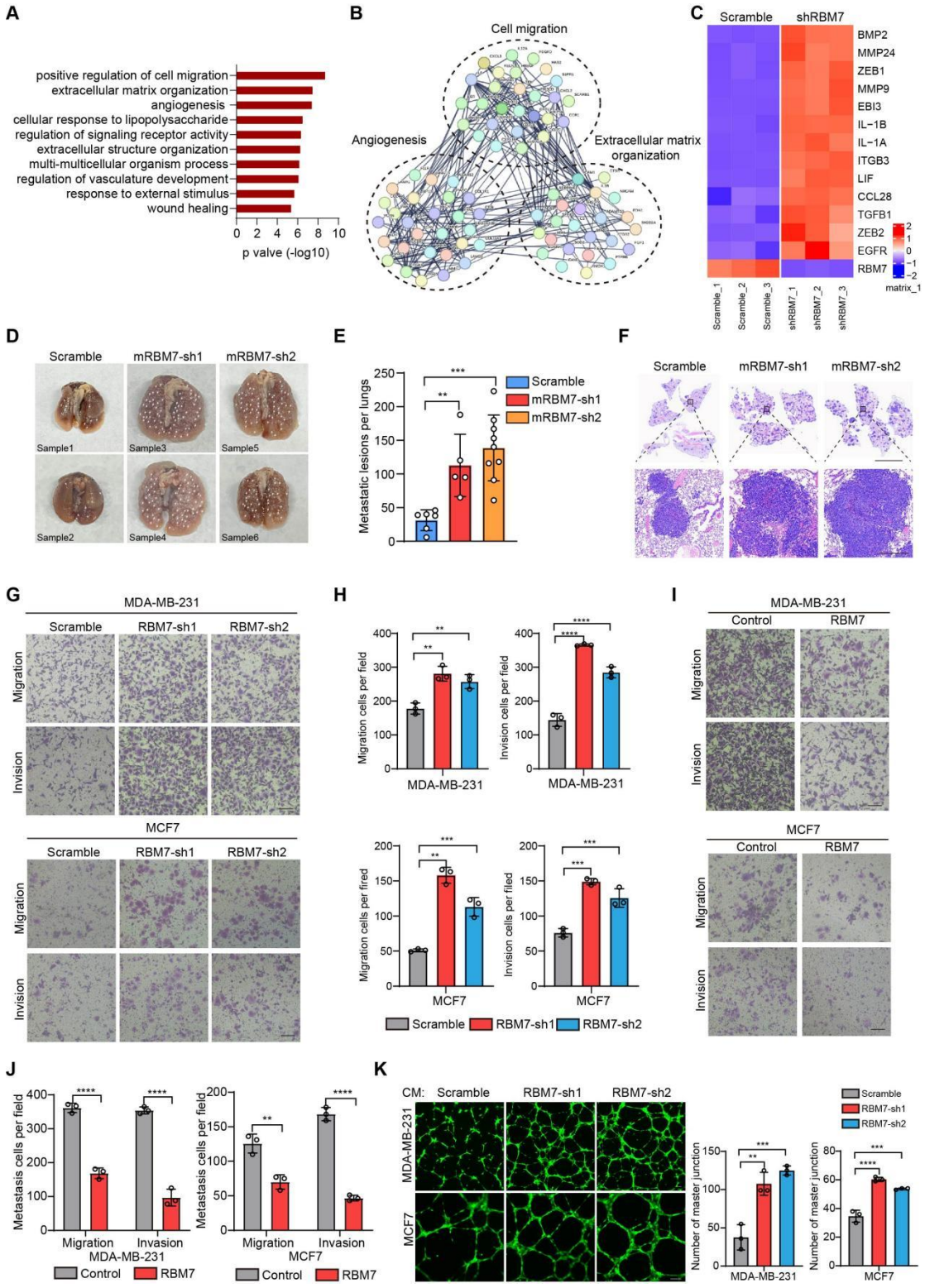

Figure 2. RBM7 negatively regulated breast cancer metastatic potential. (A) Gene Ontology analysis showed the significantly affected biological process upon RBM7 knockdown in MDA-MB-231 cells. (B) Functional association network of RBM7-regulated targets. The genes were analyzed using the STRING database, and

797 subgroups are marked according to their function. (C) A heatmap showing the
798 qRT-PCR analysis of differentially expressed genes upon RBM7 knockdown in breast
799 cancer cells from three biological replicates. (D-F) 4T1 cells without or with RBM7
800 knockdown were injected into tail vein of immunodeficient BALB/c mice to establish
801 a lung metastasis model. Spontaneous pulmonary metastases were assessed after
802 about 3 weeks, the white arrow indicates lung lesions macroscopically (D). H&E
803 stained lung sections were quantified for the number of spontaneous metastatic
804 lesions from BALB/c mice (n=6, 5 and 9). Data are presented as mean ± SD and *P*
805 values were determined by one-way ANOVA with Dunnett's multiple comparisons
806 test (E). Representative images of H&E stained lung sections are shown. Top panel
807 scale bars indicate 7 mm; bottom panel scale bars indicate 300 μm (F) . (G-J) The
808 metastatic ability of breast cancer cells with RBM7 depletion (G) or ectopic
809 expression of RBM7 (I) were evaluated by transwell assay. Scale bars: 100 μm. Data
810 are mean ± SD from three random fields. *P* values were determined by one-way
811 ANOVA with Dunnett's multiple comparisons test (H) or unpaired Student's t test (J).
812 (K) Representative images of the tube formation of HUVEC cells treated with
813 conditional medium from RBM7-KD cells or control cells for 12h. Scale bars: 100
814 μm. Quantification of number of junctions formed by HUVEC was calculated by
815 Image J software. $^{**}P < 0.01$, $^{***}P < 0.001$, $^{****}P < 0.0001$.

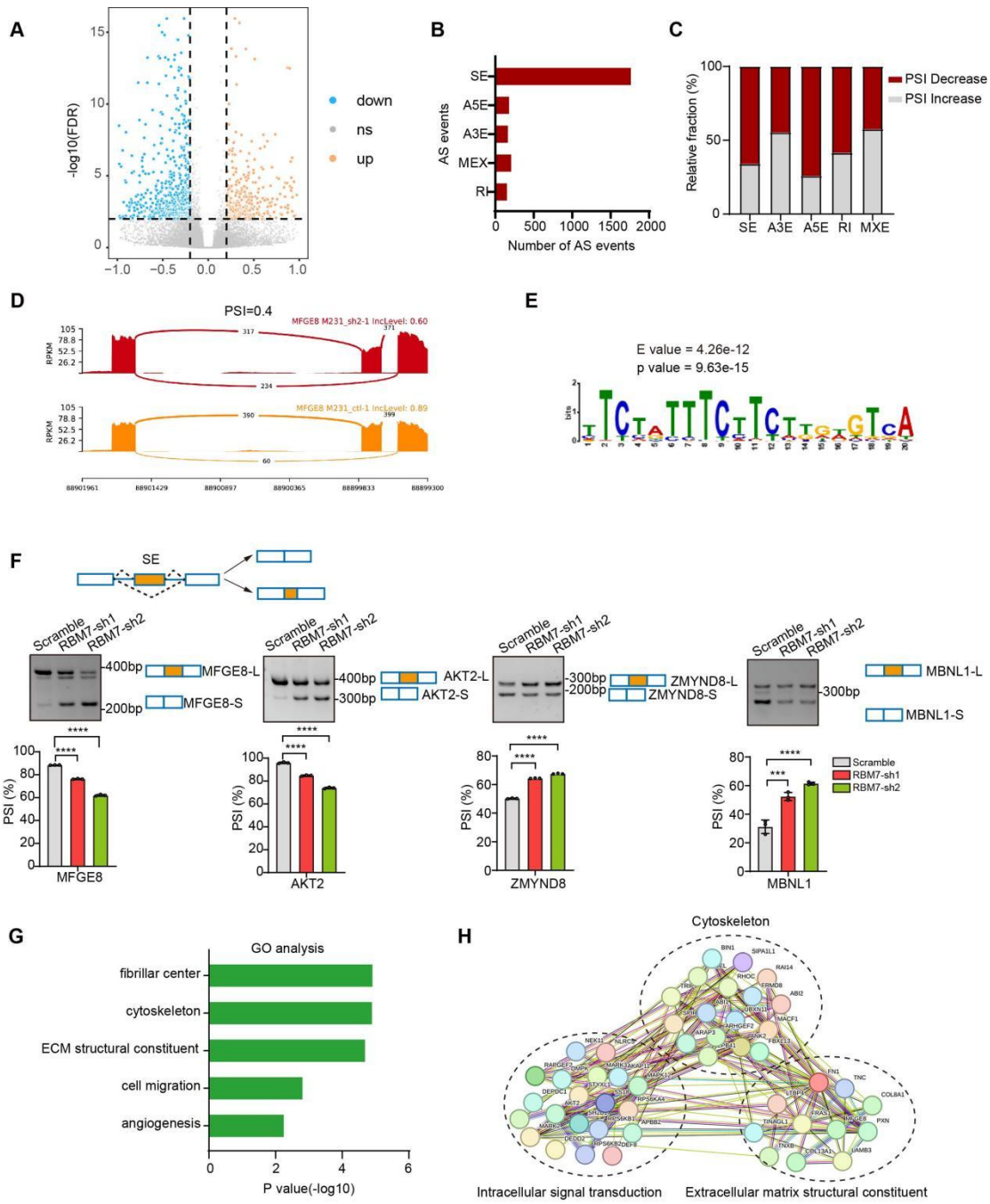

Figure 3. Global identification of alternative splicing events regulated by RBM7. (A-E) RNA-seq analysis was performed on RBM7-knockdown MDA-MB-231 cells or control cells, and the changes in splicing events were analyzed. (A) Volcano plot illustrating up-regulated/down-regulated alternative splicing events upon RBM7 depletion. (B) Comparison of the differential splicing events in five types of AS events affected by RBM7 depletion. (C) The relative fraction of splicing events undergoing percent spliced in (PSI) increase or decrease induced by RBM7 depletion. (D) Alternative splicing of MFGE8 was chosen to represent a decrease of PSI, and

825 numbers of exon junction reads were indicated. (E) The hit top enriched motifs
826 identified in the differential spliced genes regulated by RBM7. (F) RBM7-regulated
827 exon skipping events were identified by semiquantitative RT-PCR using
828 RBM7-depleted or control MDA-MB-231 cells. The mean ± SD of PSI from 3
829 independent experiments was plotted, with *P* values determined by one-way ANOVA
830 with Dunnett's multiple comparisons test. (G) Gene Ontology analysis showed the
831 significantly enriched biological processes of changed splicing events affected upon
832 RBM7 knockdown in MDA-MB-231 cells. (H) KEGG pathway enrichment analysis
833 of functional association network of the RBM7-controlled AS targets.

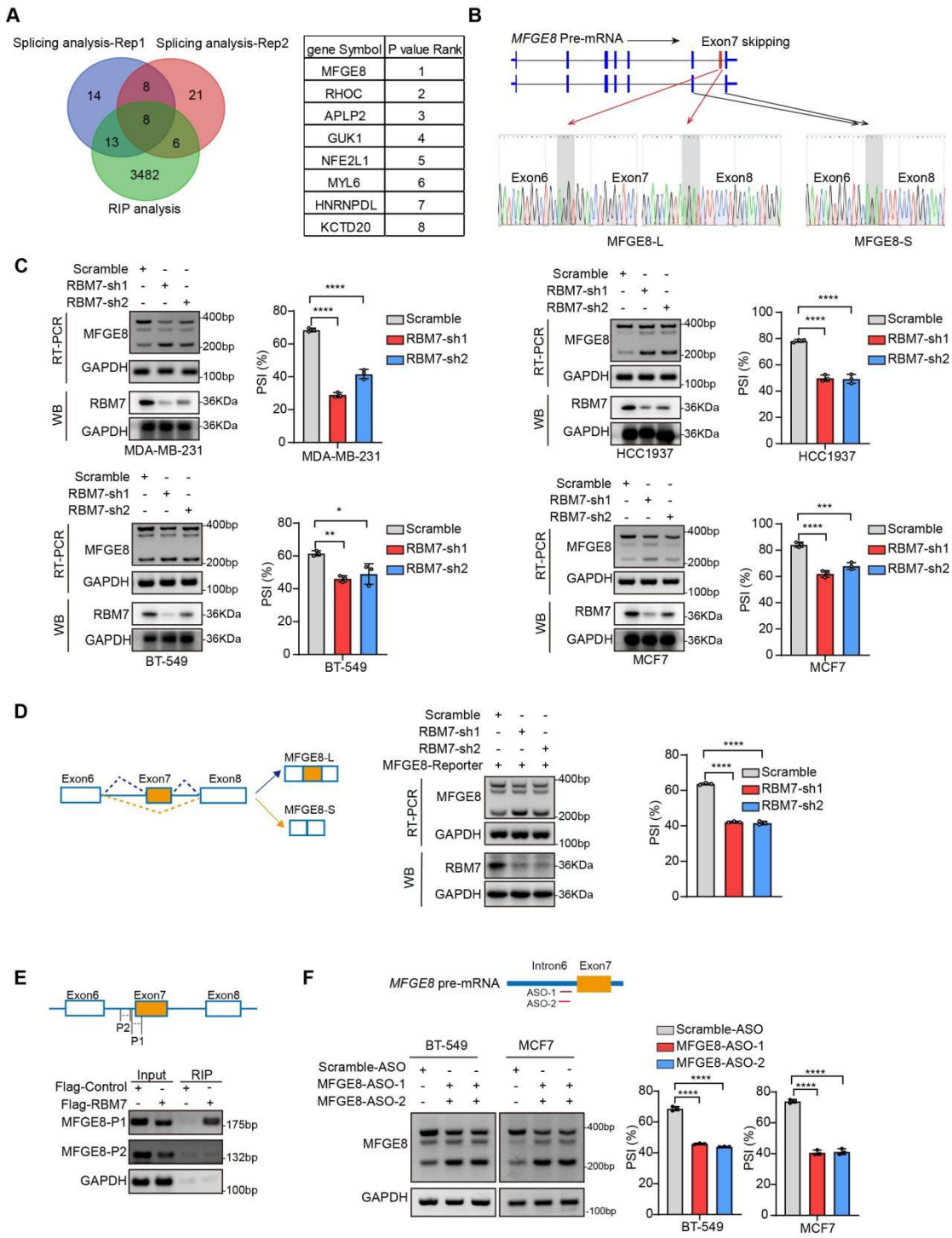

Figure 4. RBM7 knockdown promoted exon 7 skipping of MFGE8. (A) Comparison of RBM7-binding candidates from the RNA immunoprecipitation (RIP) sequencing (GSE144075 dataset) and two gene sets containing top 43 differentially AS genes in RNA-seq data of breast cancer cells expressing RBM7 shRNA1/2 as presented by venn diagram. The gene lists on the right were shown according to the FDR *P* value of top genes with significantly changed AS in RNA-seq. (B) Upper:

841 schematics of human MFGE8 pre-mRNA (NM_005928.4). MFGE8-long isoform
842 included the exon 7 (hereafter referred to as MFGE8-L), whereas it is skipped in
843 MFGE8-short isoform (hereafter referred to as MFGE8-S). The arrow indicates the
844 direction of transcription. Lower: primers were designed on exon 6/8, and RT-PCR
845 was performed to identify PSI changes using RBM7-knockdown or control
846 MDA-MB-231 cells. The base peak diagram of sanger sequencing of RT-PCR results
847 showed the splicing junction sites (filled with gray). (C) Various breast cancer cells
848 lines with stable depletion of RBM7 or control were constructed. Alternative splicing
849 events of MFGE8 regulated by RBM7 were examined by semi-quantitative RT-PCR.
850 The knockdown efficiency of RBM7 expression was detected by Western Blotting. (D)
851 Left, Schematics of MFGE8 mini-splicing reporter including exons 6-8 and two
852 flanking introns in the 600bp region upstream and downstream of 5'/3' splice sites;
853 middle, RBM7 stable knockdown or control cells were transfected with splicing
854 reporter and collected for RNA extraction after 48h. The splicing changes of
855 exogenous MFGE8 were detected by RT-PCR with specific primers on the reporter
856 gene. The level of RBM7 protein was detected in MCF7 cells by western blotting.
857 (E) As shown in schematic diagram, orange box indicates cassette exon 7 and primers
858 were designed in the putative binding regions P1 and P2. Binding of MFGE8
859 pre-mRNA with RBM7 was examined by RIP assay in HEK293T cells expressing
860 Flag-RBM7. (F) Upper: the red line in diagram indicates ASOs targeting region which
861 contain UUUCUU residues; down: MCF7 and BT-549 cells were transfected with
862 ASOs targeting MFGE8 pre-mRNA for 48h and then applied for RT-PCR
863 identification. The mean ± SD of PSIs from three repeated experiments were plotted
864 with *P* value calculated by one-way ANOVA with Dunnett's multiple comparisons test.
865 *$P < 0.05$, **$P < 0.01$, ***$P < 0.001$, and ****$P < 0.0001$.

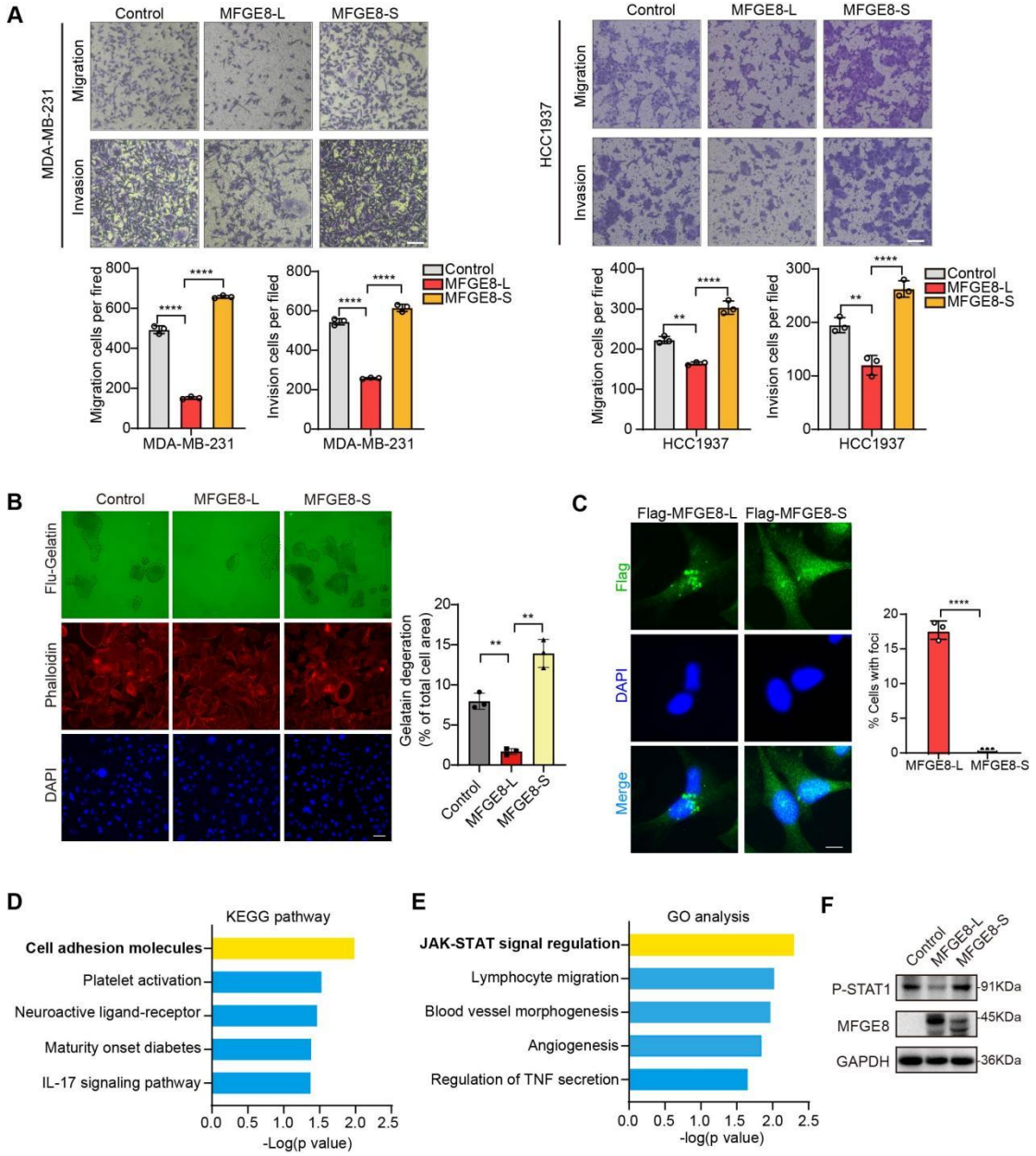

Figure 5. MFGE8-L inhibited breast cancer cell migration and invasion. (A) The function of MFGE8-L/S on breast cancer cell migration and invasion were evaluated by transwell assays. (B) Gelatin degradation assay was performed to test the effect of RBM7 knockdown on invadopodia function. 10000 cells were plated onto FITC-gelatin substrates (Green) and cultured for 48 h. Representative images are shown (red, Cy3-phalloidin; blue, DAPI) and the degraded areas were quantified by Image J software. Scar bars= 50 μm. (C) The subcellular localizations of MFGE8 isoforms. MDA-MB-231 cells were transfected with Flag-tagged MFGE8-L or MFGE8-S, and visualized with immunofluorescence assay. Scale bar = 10 μm. The percent of cells with foci were quantified and plotted (about 80 cells were captured

877 and quantified in both samples). (D-E) The KEGG pathway and Gene ontology
878 analysis of genes up-regulated by MFGE8-S compared with MFGE8-L. (F) The
879 expression levels of p-STAT1(Tyr701) in HCC1937 cells overexpressing MFGE8-L/S
880 was detected by western blotting. *P* values were determined by one-way ANOVA with
881 Tukey's multiple comparisons test. $^{**}P < 0.01$, $^{****}P < 0.0001$.

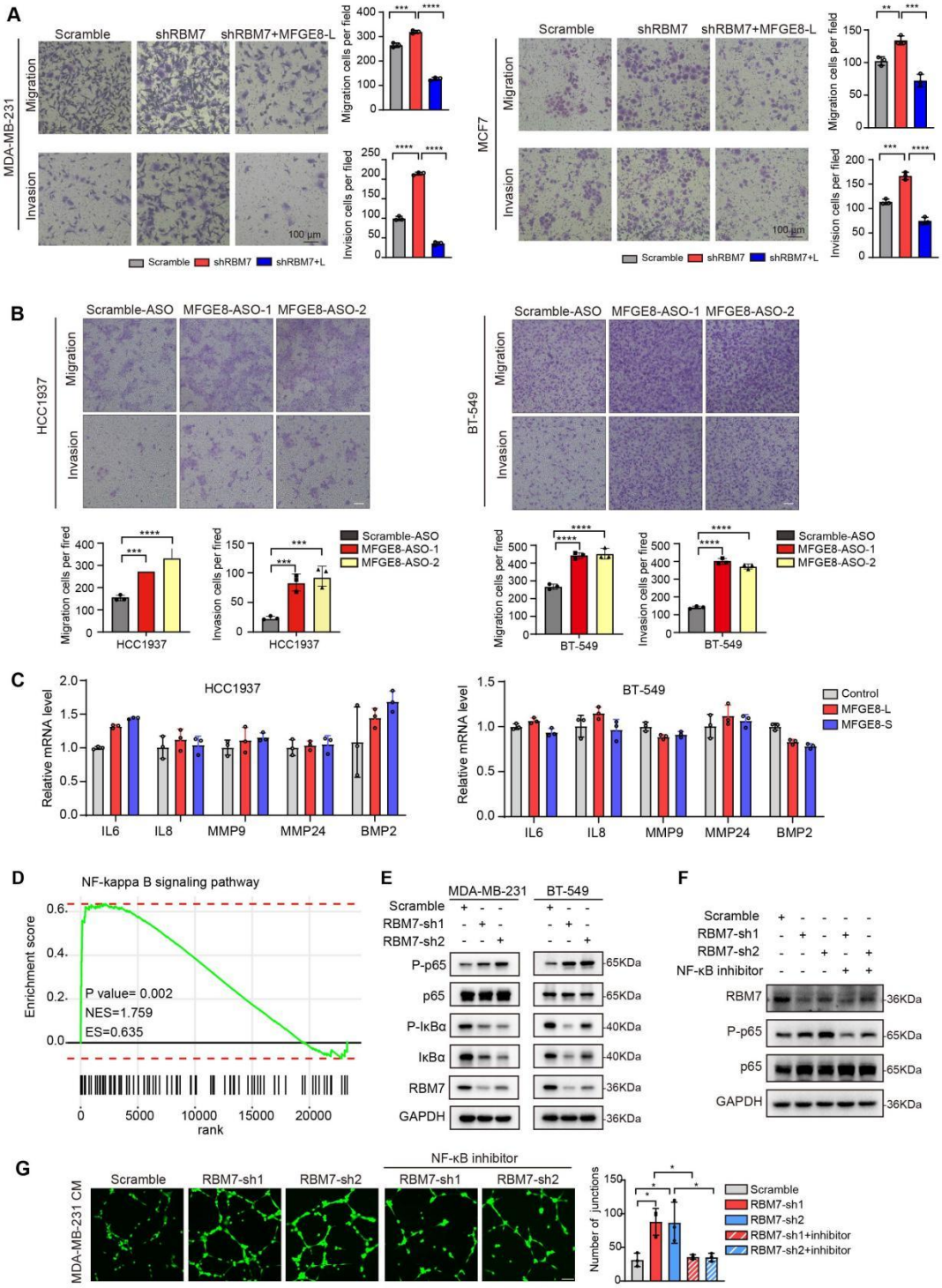

Figure 6. RBM7 knockdown enhanced aggressiveness of breast cancer relying on MFGE8 splicing switch to the short variant and NF-κB pathway activation. (A) Breast cancer cells MDA-MB-231 and MCF7 were cotransfected with shRNA targeting RBM7 and shRNA-resistant Flag-MFGE8-L vectors and then subjected to

887 transwell migration assay or invasion assay. Migrated or invaded cells were counted
888 from random sites of the transwell with Image J. (B) Representative transwell analysis
889 of migrative/invasive capability of breast cancer cells transfected with 500 nM ASO
890 directed against RBM7-binding region in MFGE8 pre-mRNA. Cells migrating
891 through transwell membrane with matrigel or not were imaged and representative
892 images are shown (upper) along with quantification (down). (C) The expression of
893 metastasis-related factors in HCC1937 and BT-549 cells stably expressing MFGE8-L,
894 MFGE8-S or control vector was measured by real-time PCR assay. (D) NF-κB
895 signaling pathway was enrichment via KEGG analysis in RBM7 knockdown breast
896 cancer cells. (E) Western blotting showed the expression of p65, P-p65, IκBα and
897 P-IκBα in NF-κB pathway in RBM7-depleted or control MDA-MB-231 and BT-549
898 breast cancer cells. (F) Western blotting was performed to test the expression of
899 RBM7, p65 and P-p65 in RBM7-depleted MDA-MB-231 cells treated with or without
900 NF-κB inhibitor PDTC 10 μm for 48h. (G) Representative images of the tube
901 formation of HUVEC cells treated with conditional medium from RBM7-depleted
902 MDA-MB-231 in the presence or absence of 10 μm NF-κB inhibitor PDTC. Scale
903 bars: 100 μm. Quantification of junctions of endothelial network was conducted by
904 ImageJ software. *P* values were determined by one-way ANOVA with Tukey's
905 multiple comparison test (n = 3). $^{*}P < 0.05$, $^{**}P < 0.01$, $^{***}P < 0.001$, and $^{****}P$
906 < 0.0001.

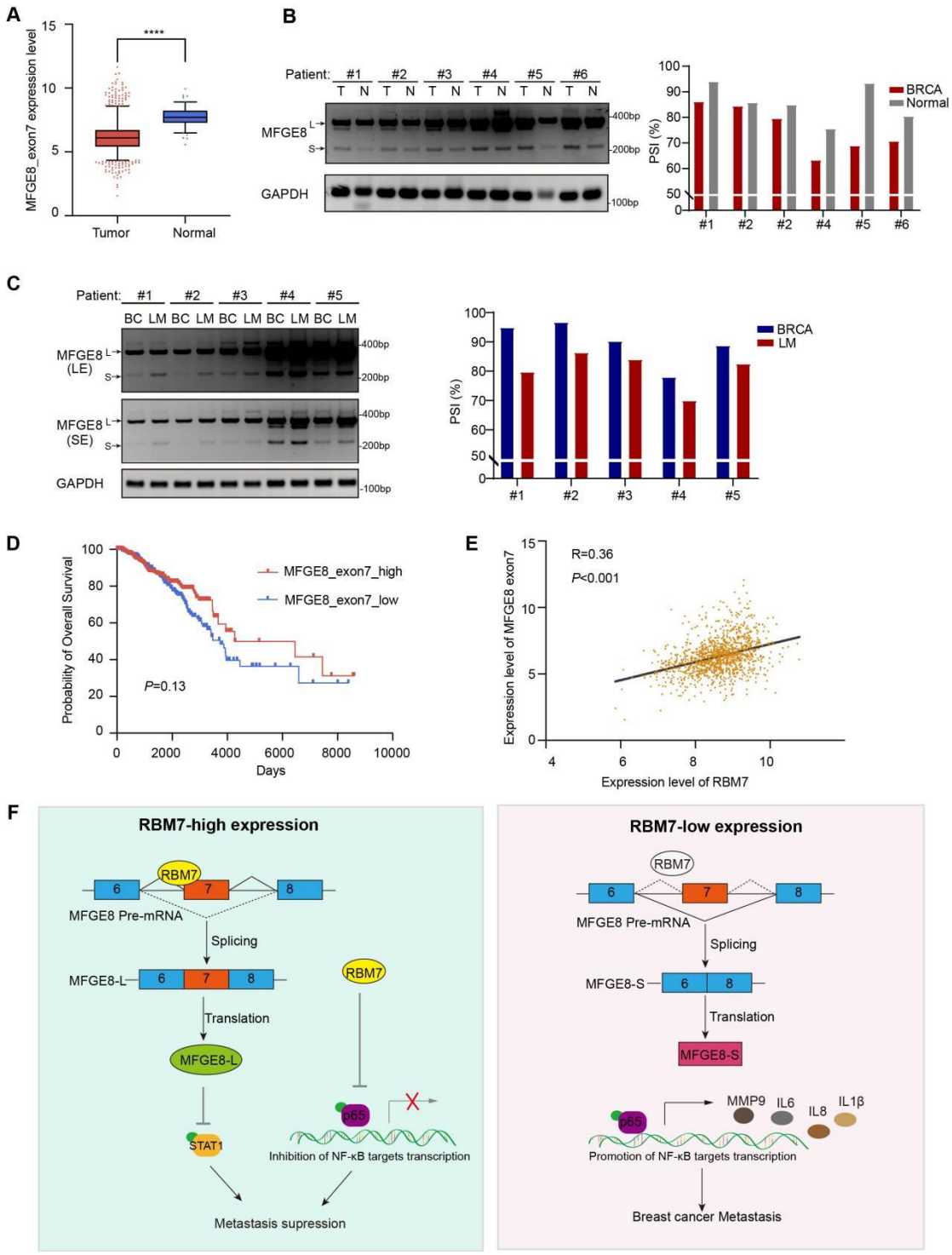

Figure 7. Splicing shift of MFGE8 toward exon7 exclusion was negatively correlated with RBM7 expression in patients with breast cancer. (A) MFGE8 exon7 expression level was analyzed in breast carcinoma in comparison with normal tissues based on the TCGA dataset. Plotted are the mean ± SD from 114 normal tissues and 1094 tumor tissues, with **** $P<0.0001$ as determined by unpaired

913 Student' t test. (B) The splicing alteration of MFGE8 in 6 pairs of primary breast
914 cancer tissues and adjacent normal tissues was examined using RT-PCR.The
915 quantification of PSI vales was based on relative band intensities using Image J
916 software. (C) The splicing alteration of MFGE8 in primary breast cancer tissues and
917 corresponding lymph node metastases was identified by RT-PCR assays. The
918 quantification of PSI vales was determined by Image J software. (D) The correlation
919 between the expression of MFGE8 exon7 and overall survival (OS) of breast cancer
920 patients was analyzed based on the TCGA dataset. *P* value was assessed with
921 Mantel-Cox log-rank test. (E) Correlation of RBM7 expression with MFGE8 exon7
922 levels was analyzed using Pearson's correlation coefficient method. (F) The
923 mechanistic model of how RBM7 regulated metastasis of breast cancer through
924 regulating MFGE8 splicing switch.